

# 1            **Significant Production of Ozone from Germicidal UV Lights at 222 nm**

2  
3    Zhe Peng,<sup>1,2</sup> Douglas A. Day,<sup>1,2</sup> Guy Symonds,<sup>1,2</sup> Olivia Jenks,<sup>1,2</sup> Harald Stark,<sup>1,2,3</sup> Anne V.  
4    Handschy,<sup>1,2</sup> Joost de Gouw,<sup>1,2</sup> and Jose L. Jimenez<sup>1,2</sup>

5  
6    1: Dept. of Chemistry, University of Colorado, Boulder, CO, USA

7    2: Cooperative Institute for Research in Environmental Sciences (CIRES), University of  
8    Colorado, Boulder, CO, USA

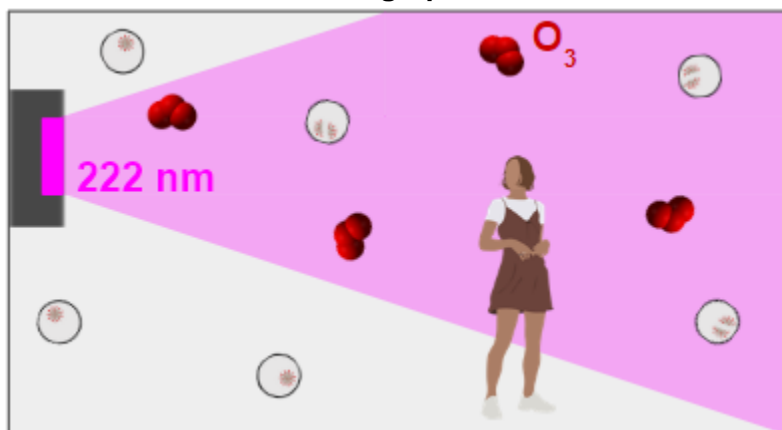
9    3: Aerodyne Research, Billerica, MA, USA

---

## 11            **Abstract**

12  
13  
14  
15    Lamps emitting at 222 nm have attracted recent interest for germicidal ultraviolet disinfection  
16    (“GUV222”). Their impact on indoor air quality is considered negligible. In this study, ozone  
17    formation is observed for eight different lamps from five manufacturers, in amounts an order-of-  
18    magnitude larger than previous reports. Most lamps produce O<sub>3</sub> in amounts close to the first-  
19    principles calculation, with e.g. a generation rate of 22 ppb h<sup>-1</sup> for Ushio B1 modules in a 21 m<sup>3</sup>  
20    chamber. Much more O<sub>3</sub> is produced by lamps when optical filters were removed for tests, and  
21    by an undesired internal electrical discharge. A test in an office shows an increase of ~6.5 ppb  
22    during lamp-on periods, consistent with a simple model with the O<sub>3</sub> generation rate, ventilation  
23    and O<sub>3</sub> losses. We demonstrate the use of a photolytic tracer to quantify the averaged GUV222  
24    fluence rate in a room. Low-cost electrochemical O<sub>3</sub> sensors were not useful below 100 ppb.  
25    Formation of O<sub>3</sub> increases indoor particulate matter (PM), which is ~10-30 times more deadly  
26    than O<sub>3</sub> per unit mass, and which is ignored when only considering O<sub>3</sub> threshold limit values. To  
27    limit GUV222-created indoor pollution, lower fluence rates should be used if possible, especially  
28    under low-ventilation conditions.

29  
30            **TOC graphic:**



## 33 1. Introduction

34  
35 Germicidal ultraviolet (GUV) disinfection has been used for a century to inactivate airborne  
36 pathogens, i.e. those that infect via inhalation of pathogen-containing aerosols that float in the  
37 air.<sup>1-3</sup> Despite some early interest in widespread deployment (e.g. a campaign from  
38 Westinghouse to install GUV lamps in every American home<sup>4</sup>), it has remained mostly a niche  
39 technique in medical circles, in particular to reduce tuberculosis transmission.<sup>5</sup> Research during  
40 the COVID-19 pandemic led to the conclusion that airborne transmission is dominant for this  
41 virus,<sup>6</sup> and also important for other respiratory viruses.<sup>7</sup> This has resulted in intense interest in  
42 methods to remove pathogens from the air, including ventilation, filtration, and air disinfection, in  
43 particular by GUV.<sup>8</sup>

44  
45 GUV uses lamps that emit light in the UVC range (200-280 nm) to irradiate indoor air, which can  
46 inactivate aerosol-bound pathogens. It has traditionally been performed using filtered mercury  
47 lamps whose most intense emission is at 254 nm (“GUV254”). More recently the use of shorter  
48 wavelengths (“far UVC”, 200-230 nm) has gained in popularity, in particular using KrCl excimer  
49 with peak emission of 222 nm (“GUV222”). Extensive scientific reference information on GUV  
50 has been compiled at the online GUV Cheat Sheet.<sup>9</sup>

51  
52 UVC lamps with wavelengths below 242 nm can generate O<sub>3</sub>,<sup>10</sup> a dangerous pollutant. A recent  
53 review concluded that O<sub>3</sub> generation by KrCl lamps was minimal: for example a 12 W lamp was  
54 estimated to take 267 h to produce 4.5 ppb O<sub>3</sub> in a 30 m<sup>3</sup> room in the absence of losses.<sup>11</sup> A  
55 recent modeling paper estimated O<sub>3</sub> generation to be nearly two orders-of-magnitude faster,<sup>12</sup>  
56 but those findings have not been confirmed experimentally. There is also discussion in the  
57 literature whether O<sub>3</sub> is mainly formed by the UVC radiation or by discharges in electrical  
58 connections.<sup>11</sup>

59  
60 In addition, it is typically difficult to quantify the GUV fluence rate that the air experiences in a  
61 room or chamber, since lamp emission results in inhomogeneous light spatial distributions, the  
62 reflectivity of materials at the GUV wavelengths varies widely, and due to continuous and highly  
63 variable air motion. Measurements in different points of a room to quantify the average, or  
64 computer modeling can be performed but are time consuming. Quantification of the radiation  
65 field with measurements of inactivation of viruses or bacteria require culture assays which are  
66 slow and very costly.

67  
68 Here we present direct measurements of O<sub>3</sub> production from KrCl excimer lamps in a laboratory  
69 chamber and compare them with literature estimates. A chemical tracer that allows  
70 quantification of GUV fluence rate is introduced. Measurements are also performed in an office.  
71 Significant O<sub>3</sub> production is observed in both controlled-laboratory and real-world settings.

## 72 2. Methods

### 73 *Demonstration of tracers for GUV exposure of air*

74  
75  
76

77 In this work, we use  $\text{CBr}_4$  as a chemical tracer of GUV exposure. We show that it has relatively  
78 fast decay under 222 nm irradiation and can be detected by commonly-available Proton-  
79 Transfer-Reaction Mass Spectrometers with high sensitivity. It does not react with common  
80 atmospheric oxidants such as  $\text{O}_3$ , OH, or  $\text{NO}_3$  at typical indoor air concentrations. It has high  
81 vapor pressure and low water solubility which minimizes partitioning to room surfaces and  
82 tubing.<sup>13,14</sup> More details can be found in Section S1.

83

### 84 **Laboratory chamber experiments**

85

86 A well-characterized environmental chemical reaction chamber was used to measure the  $\text{O}_3$   
87 production rate and  $\text{CBr}_4$  tracer decay for individual GUV fixtures. A  $\sim 21 \text{ m}^3$  Teflon reaction  
88 chamber (approximately 3x3x2 meters, LxWxH) is constructed of 50  $\mu\text{m}$  thick FEP Teflon film  
89 (ATEC, Malibu, California). Temperature during the experiments was  $\sim 20\text{-}25^\circ\text{C}$ , and the built-in  
90 chamber UVA / visible lights were not used other than at occasional low-levels of visible lights  
91 for task lighting. The chamber systems are described in previous publications exploring  
92 chemical and physical processes of gases and aerosols.<sup>15,16</sup> The GUV light source was placed  
93 either a few cm outside the chamber (at one corner shining into the bag and diagonally across  
94 to the opposite corner at mid-height) or placed within the chamber (at a lower corner mounted  
95 on a ring stand facing the opposite upper corner) (Fig. S1).

96

97 A typical experiment was conducted as follows. Prior to each experiment, the chamber was  
98 flushed for several hours with 400 LPM clean air ( $\text{NO}_x < 0.2 \text{ ppb}$ ;  $\text{VOC} < 50 \text{ ppb}$ ) from an AADCO  
99 generator (Model 737-15A) (at slightly positive pressure, 1-2 Pa) and then topped off to  
100 consistently reach the full volume ( $\sim 21 \text{ m}^3$ ) by filling until the differential pressure reached 3.5  
101 Pa. The GUV lamp was then turned on either continuously (Fig. 1b) or on/off in steps (e.g., 120  
102 minutes on, 45 minutes off, Fig. 1a) for several hours.  $\text{O}_3$  formation was measured with a  
103 Thermo Scientific 49i  $\text{O}_3$  Analyzer. Later in the experiments while the GUV lamp was off, several  
104 ppb of  $\text{CBr}_4$  were added by placing the solid compound within a glass bulb and gently heating  
105 with a heat gun while flowing UHP nitrogen gas (for  $\sim 2$  minutes), and then mixing for 1 minute  
106 with a Teflon-coated mixing fan (integrated in the chamber). The on/off operation allowed to  
107 unequivocally attribute changes in the  $\text{O}_3$  and  $\text{CBr}_4$  mixing ratios to the GUV illumination, and to  
108 quantify any other losses separately.  $\text{CBr}_4$  was measured with Vocus (detected as  $\text{CBr}_3^+$ ), which  
109 was calibrated by adding a known quantity to the chamber.<sup>17</sup> See Sections S2 and S3 for more  
110 information on calibrations of the  $\text{O}_3$  analyzers and Vocus.

111

112 Since a single lamp fixture was illuminating from one corner of the bag, the fluence rate is not  
113 constant within the bag volume. However, on the timescales of the experiments (relative to the  
114 production/decay of the measured compounds), the air within the chamber is relatively well  
115 mixed. This is due to the continuous mixing that occurs in the absence of mechanical mixing,  
116 with a timescale of  $\sim 10$  minutes.<sup>16</sup> This is apparent in the stepwise lamp illumination  
117 experiments, by the relatively quick stabilization of  $\text{CBr}_4$  and  $\text{O}_3$  when the light is turned off (Fig.  
118 1a).

119

120 Table 1. KrCl excimer lamps tested in the chamber experiments and key results. Also shown are the results of first-principles  
 121 calculations with different lamp spectra.  
 122

Manufacturer	Model	Spectrum or Lamp	Inside or Outside Teflon Bag?	Filtered?	Electrical power (W)	O <sub>3</sub> generation rate (ppb h <sup>-1</sup> )	CBr <sub>4</sub> photolysis rate (h <sup>-1</sup> )	Ratio between the 2 rates (ppb)	O <sub>3</sub> generated per unit power μg h <sup>-1</sup> W <sup>-1</sup>	Effective fluence rate (μW cm <sup>-2</sup> s <sup>-1</sup> )
N/A		Theoretical calculation w/ narrow emission line at 222 nm <sup>a</sup>				14	0.11	130		2.1
N/A		Theoretical calc. w/ Ushio B1 (NIST-measured spectrum) <sup>a</sup>				22	0.097	230		2.1
N/A		Theoretical calc. w/ Ushio B1 (NIST spectrum, adding an estimated 190 nm band) <sup>b</sup>				88	0.097	910		2.2
Far UV	Krypton -36	Ushio B1	Inside	Yes	15	21	0.093	230	48	2.0
Far UV	Krypton -36	Ushio B1	Inside	No - removed by us	15	100	0.21	490	230	4.6
Far UV	Krypton -36	Ushio B1	Outside	No - removed by us		66				
Custom	N/A	Ushio B1	Inside	Yes	16	23	0.10	230	49	2.2
Custom	N/A	Ushio B1.5 (with diffuser)	Inside	Yes	11	8.5	0.051	170	26	1.1

Naomi Wu, China	N/A	GMV FAR-UVC 15 W	Inside	Yes	15	11	0.039	280	25	0.84
Naomi Wu, China (portable)	N/A	FIRST UVC HEXAGON - USB	Inside	Yes	5	2.0	0.0095	210	7	0.21
ERGO HealthTech	X One	Not known	Inside	Yes	5	2.0	0.0081	250	13	0.18
Eden Park (A)	MobileShield <sup>222</sup>	Eden Park Microplasma Far-UVC	Inside	Yes	9	30	0.030	1000	110	0.65
Eden Park (A)	MobileShield <sup>222</sup>	Eden Park Microplasma Far-UVC	Inside	No - removed by us	9	70	0.040	1800	260	0.86
Eden Park (A)	MobileShield <sup>222</sup>	Eden Park Microplasma Far-UVC	Outside	No - removed by us		0.51				
Eden Park (B)	MobileShield <sup>222</sup>	Eden Park Microplasma Far-UVC	Inside	Yes	9	1.3	0.010	120	4.6	0.22
Eden Park (B)	MobileShield <sup>222</sup>	Eden Park Microplasma Far-UVC	Inside	No - removed by us	9	14	0.039	360	52	0.84

123 <sup>a</sup> hypothetical case with a total UV intensity of  $2.3 \times 10^{12}$  photons  $\text{cm}^{-2} \text{s}^{-1}$

124 <sup>b</sup> hypothetical case with the same 222 nm band as the NIST-measured Ushio B1 spectrum and an artificial 190 nm band, constructed from the

125 spectrum shown in ref.<sup>11</sup> (Fig. S2)

## 126 **Office experiments**

127  
128 Experiments were also performed in a small university office, which measured 4.0x2.7x3.1 m  
129 (LxWxH; vol. ~33 m<sup>3</sup>). It has an entrance door and two windows. A supply and a return vent are  
130 located near the ceiling. To simulate a low-ventilation situation, the windows, gaps around utility  
131 penetrations, and supply / return vents were sealed with plastic sheeting or tape (Fig. S3).

132  
133 The ventilation rate was quantified by monitoring the decay of CO<sub>2</sub> after an injection (from a  
134 compressed gas cylinder) with an Aranet4 sensor (SAFTehnika, Latvia). A fan was turned on  
135 remotely for a few seconds after CO<sub>2</sub> injection to ensure homogeneity within the room. The  
136 ventilation / infiltration rate was estimated with an exponential fit to the CO<sub>2</sub> decay to be as low  
137 as ~0.44 h<sup>-1</sup> (timescale of ~2.3 h, comparable to typical residences),<sup>18</sup> but with some  
138 experiment-to-experiment variability. For this reason CO<sub>2</sub> was injected also during the O<sub>3</sub> decay  
139 or production experiments.

140  
141 To quantify the O<sub>3</sub> decay to surfaces and to gas and aerosol chemistry in the room, the O<sub>3</sub>  
142 decay in the room was measured with a 2B 205 analyzer. The decay was fit to an exponential,  
143 and the O<sub>3</sub> deposition rate coefficient was determined by subtracting the ventilation rate  
144 coefficient (Fig. S4).

## 145 **3. Results**

### 146 ***Theoretical estimation of O<sub>3</sub> production and tracer decay***

147  
148 In this study, we tested lamps from different manufacturers (Table 1). The emission spectrum of  
149 the Ushio B1 lamp that is used by multiple lamp manufacturers is available from NIST (Fig. S2).  
150 The absorption spectra of O<sub>2</sub> and CBr<sub>4</sub> are well-known.<sup>10,19</sup> Their expected photolysis rates  
151 under the Ushio B1 lamp irradiation can be calculated by integrating the product of UV fluence  
152 rate and absorption cross sections of O<sub>2</sub> or CBr<sub>4</sub> over the wavelengths of interest. As 2  
153 molecules of O<sub>3</sub> are produced per O<sub>2</sub> molecule photolyzed, the theoretical O<sub>3</sub> production rate for  
154 the Ushio B1 lamp at a total UV fluence rate of 2.3x10<sup>12</sup> photons cm<sup>-2</sup> s<sup>-1</sup> is ~22 ppb h<sup>-1</sup>. At the  
155 same UV intensity, the theoretical CBr<sub>4</sub> photolysis rate is 0.097 h<sup>-1</sup>. The ratio between them  
156 (P<sub>O<sub>3</sub></sub>/J<sub>CBr<sub>4</sub></sub> ~ 230 ppb), i.e. O<sub>3</sub> production through O<sub>2</sub> photolysis over a period for an e-fold decay  
157 of CBr<sub>4</sub>, is independent of UV fluence rate and is characteristic of a specific GUV222 lamp.

158  
159  
160  
161 When unfiltered optically, the emission of KrCl excimer lamp also includes a band centered at  
162 190 nm (Fig. S2).<sup>11</sup> If this band is added to the theoretical calculation (as a proxy of unfiltered  
163 lamps), the O<sub>3</sub> generation rate is increased by a factor of ~4. Although the 190 nm band has  
164 much lower intensity, the absorption cross section of O<sub>2</sub> is on average ~2 orders of magnitude  
165 larger for the 190 nm band than for the 222 nm one. However, this band has little impact on  
166 CBr<sub>4</sub> as its cross section below 200 nm is much lower. This results in a higher P<sub>O<sub>3</sub></sub>/J<sub>CBr<sub>4</sub></sub> ratio  
167 (~900 ppb) than for the filtered lamp spectrum.

### 168 ***O<sub>3</sub> production and CBr<sub>4</sub> in the chamber***

170  
171 Results of a typical chamber experiment (Ushio B1) are shown in Fig. 1a. O<sub>3</sub> increases  
172 approximately linearly with time when the lamp is on. When this lamp is on for an extended  
173 period (days), O<sub>3</sub> in the chamber can reach ppm levels (Fig. S5). At very high O<sub>3</sub>  
174 concentrations, the small loss rate coefficient of O<sub>3</sub> (mainly due to O<sub>3</sub> photolysis by the 222 nm  
175 band, Fig. S6) slightly reduces the rate of O<sub>3</sub> increase. An Ushio B1 lamp generates ~22 ppb O<sub>3</sub>  
176 per h, very close to the theoretical case shown above. The effective UVC fluence rate inferred  
177 from the CBr<sub>4</sub> photolytic decay rate (~0.1 h<sup>-1</sup>, dilution corrected, Table 1) (Fig. 1b), is also very  
178 close to the theoretical case value. P<sub>O<sub>3</sub></sub>/J<sub>CBr<sub>4</sub></sub>, a characteristic of the lamp, is almost the same as  
179 the theoretical case value (Table 1).

180  
181 The other devices tested in this study, with electrical power ranging from ~5 W (portable device)  
182 to ~15 W, also have P<sub>O<sub>3</sub></sub>/J<sub>CBr<sub>4</sub></sub> values in the range of 200-300 ppb, indicating similar spectral  
183 characteristics of their emissions. The exceptions are the lamps whose filters were removed for  
184 our tests, two Eden Park lamps we tested, and an Ushio B1.5 lamp with a diffuser.

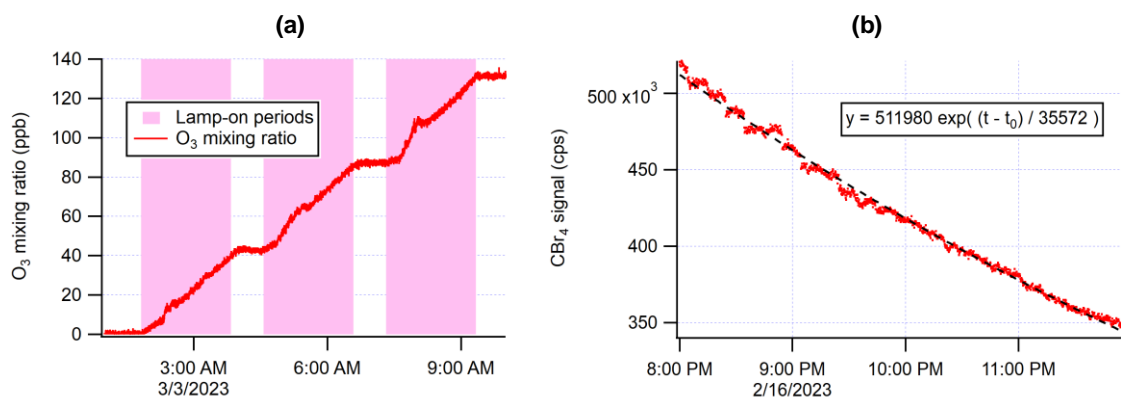
185  
186 The Far UV device with filter removed has 4 times more O<sub>3</sub> production and >100% larger CBr<sub>4</sub>  
187 decay than when it has the filter, leading to about twice P<sub>O<sub>3</sub></sub>/J<sub>CBr<sub>4</sub></sub> of the device with the filter.  
188 Without the filter, more photons of the 222 nm band are allowed out of the device, leading to  
189 faster CBr<sub>4</sub> decay. The 190 nm band is also unfiltered, producing much more O<sub>3</sub> than the 222  
190 nm band of the device without filter can produce.

191  
192 The Eden Park lamp has almost the same emission spectrum as the Ushio B1 (Fig. S7). With its  
193 filter, the first Eden Park device tested (EP-A, Table 1) results in ~1/3 CBr<sub>4</sub> decay vs. Ushio B1,  
194 while producing more O<sub>3</sub>. Most of this unexpectedly high O<sub>3</sub> production appears to be due to  
195 electrical discharge within the electrical components of the device (but outside the lamp). We  
196 arrive at this conclusion after additional tests: (i) low O<sub>3</sub> production by the EP-A in the chamber  
197 bag when located outside the bag, in contrast to the Ushio B1 module (Table 1). (ii) For O<sub>3</sub>  
198 measurement just outside the EP-A housing, but not in front of the light, the O<sub>3</sub> monitor detects  
199 ppm-level O<sub>3</sub> (Fig. S8), implying very strong non-photochemical O<sub>3</sub> production inside the device.

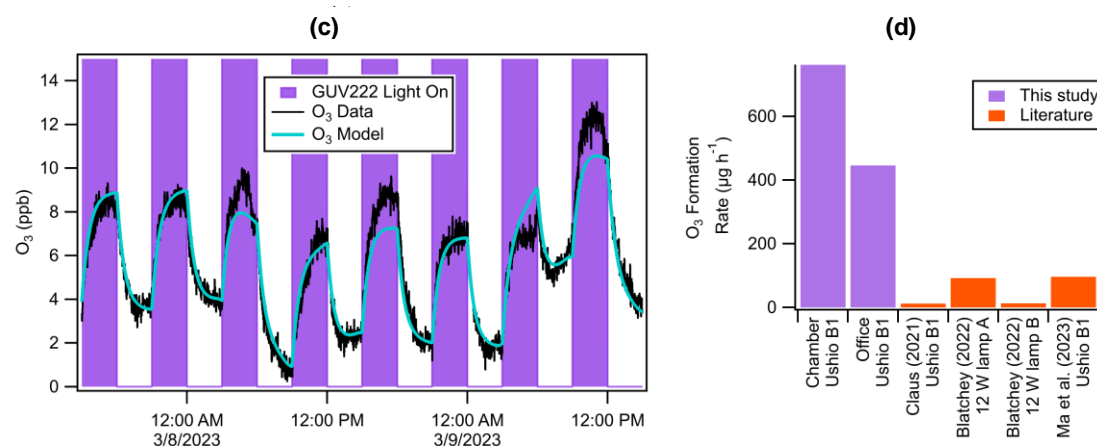
200  
201 In contrast, the other Eden Park device test (EP-B) did not produce an excessive amount of O<sub>3</sub>  
202 in its housing, implying no undesired electrical discharge there. It also only produces 1.3 and 14  
203 ppb O<sub>3</sub> per h in the chamber with and without its filter, respectively, resulting in significantly  
204 lower P<sub>O<sub>3</sub></sub>/J<sub>CBr<sub>4</sub></sub> than the Ushio B1 lamps. The reasons for the lower P<sub>O<sub>3</sub></sub>/J<sub>CBr<sub>4</sub></sub> of the Ushio B1.5  
205 module and EP-B lamp are unclear, as they have similar emission spectra to Ushio B1 (Fig.  
206 S7).

207

208



209  
210



211  
212 *Figure 1. Time series of (a) O<sub>3</sub> and (b) CBr<sub>4</sub> during chamber experiments with the 12 W Far UV*  
213 *lamp (Ushio B1 module). (c) Time series of O<sub>3</sub> in the office experiments, along with model*  
214 *results. (d) Comparison of O<sub>3</sub> formation rates in this study with previous literature.*

215

### 216 **O<sub>3</sub> mass balance in an office**

217

218 The Far UV lamp was repeatedly cycled on (3 h) and off (3 h) together with periodic CO<sub>2</sub>  
219 injections (Fig. 1c and Fig. S9). O<sub>3</sub> rapidly rose once the lamp was turned on and reached an  
220 approximate steady state (8-14 ppb, typically increasing ~6.5 ppb). After turning off the lamp, O<sub>3</sub>  
221 rapidly decreased, also quickly reaching a steady state. Background O<sub>3</sub> in the office, as  
222 indicated by the steady-state O<sub>3</sub> level at the end of lamp-off periods, varied by ~4 ppb during the  
223 experiment. It is affected by ventilation rate, deposition, as well as O<sub>3</sub> in outdoor/adjacent-room  
224 air infiltrating into the office. Ventilation rates ranged 0.62-0.96 h<sup>-1</sup> (Fig. S9). O<sub>3</sub> deposition rates  
225 were more variable (range 0.5-2.3 h<sup>-1</sup>, average 0.78 h<sup>-1</sup>, Fig. S9).

226

227 O<sub>3</sub> in the office was modeled with a chemical-kinetics simulator.<sup>20</sup> The model was constrained  
228 by the measured O<sub>3</sub> and CO<sub>2</sub> concentrations and decays (Section S4). The measured and  
229 modeled O<sub>3</sub> are in good agreement (Fig. 1c). The O<sub>3</sub> production rate of the Ushio B1 module in  
230 the office (Fig. S3) is estimated to be 8.6 ppb/h from the constrained model. This is ~39% of the  
231 value measured in the chamber, which is explained by the larger volume of the office (~32.9 vs.  
232 ~20.6 m<sup>3</sup>) and the shorter effective UV pathlength (~3.2 vs. ~4.5 m). Scaling results in a  
233 difference of 12%, thus showing agreement well within experimental uncertainties (Fig. S10).

## 234 **Implications**

235  
236 Significant amounts of O<sub>3</sub> can be produced by GUV-222 lamps in both controlled-laboratory and  
237 real-world settings. Our results of 762 µg h<sup>-1</sup> for a 21 m<sup>3</sup> chamber and 446 µg h<sup>-1</sup> for an office  
238 with a shorter light path are summarized in Fig. 1d. Note that these results would be ~18%  
239 higher at sea level due to the reduced ambient pressure in Boulder. For comparison, previous  
240 reports for the same GUV222 module (or modules using the same electrical power) from the  
241 literature of 12,<sup>11</sup> 13 and 92,<sup>21</sup> and 96 µg h<sup>-1</sup><sup>22</sup> are also shown. These had been used to  
242 conclude that O<sub>3</sub> generation from GUV222 is not a concern. On average, our results are an  
243 order of magnitude larger than the literature. The discrepancy may arise because most prior  
244 measurements were performed in small boxes, with very short optical pathlengths and high  
245 surface/volume ratios that are not representative of real room applications. The former may lead  
246 to smaller O<sub>3</sub> production rate, and the latter to substantial losses to the box surfaces, which  
247 were not accounted for. Moreover, some of these measurements may have been made with  
248 low-cost electrochemical O<sub>3</sub> sensors. We tested four sensors and found them to be  
249 unresponsive to O<sub>3</sub> mixing ratios below 200 ppb, therefore such sensors are not useful for this  
250 problem (Section S5).

251  
252 O<sub>3</sub> itself is a major air pollutant with excess deaths observed at levels below those in  
253 occupational guidelines of 50-100 ppb.<sup>23,24</sup> Critically, it can also lead to formation of other  
254 pollutants including particulate matter,<sup>12</sup> which has ~10-30 times higher excess death impacts  
255 on a mass basis (Section S6).<sup>23,25</sup> O<sub>3</sub> production by GUV222 lamps thus can be a major  
256 concern, at least under low-ventilation conditions.

257  
258 Our experiments have an average fluence rate of ~2.1 µW cm<sup>-2</sup> s<sup>-1</sup>, about 1/3 of the recently-  
259 updated ACGIH eye limit, and approximately consistent with a room installation that achieves  
260 the ACGIH limit at eye level (H. Claus, pers. comm.). ACGIH should consider reduced limits at  
261 low ventilation rates. Current literature estimates of the GUV222 disinfection rate coefficient for  
262 SARS-CoV-2 span a factor of 33.<sup>26,27</sup> Future research should focus on narrowing down this  
263 range, which may allow high efficacy of GUV222 at lower fluences, thus reducing impacts on  
264 indoor air.

## 265 **Acknowledgements**

266  
267  
268 We thank the Balvi Filantropic Fund, the CIRES Innovative Research Program, and the Sloan  
269 Foundation (grant 2019-12444) for support of this work. We thank Shelly Miller, Kenneth Wood,  
270 Ewan Eadie, Catherine Noakes, Dustin Poppendieck, Michael Link, Mikael Ehn, Jesse Kroll,  
271 Victoria Barber, John Balmes, and the larger GUV scientific and technical communities for  
272 useful discussions. We are grateful to Holger Claus, Aaron Collins, Matthew Pang, Kristina  
273 Chang, Scott Diddams and Naomi Wu for sharing data or materials and useful discussions.

274

## 275 References

- 276 (1) Wells, W. F. Air Disinfection in Day Schools. *Am. J. Public Health Nations. Health* **1943**, *33*  
277 (12), 1436–1443.
- 278 (2) Riley, R. L.; Mills, C. C.; O'grady, F.; Sultan, L. U.; Wittstadt, F.; Shivpuri, D. N.  
279 Infectiousness of Air from a Tuberculosis Ward. Ultraviolet Irradiation of Infected Air:  
280 Comparative Infectiousness of Different Patients. *Am. Rev. Respir. Dis.* **1962**, *85*, 511–525.
- 281 (3) Nardell, E. A. Air Disinfection for Airborne Infection Control with a Focus on COVID-19:  
282 Why Germicidal UV Is Essential†. *Photochem. Photobiol.* **2021**, *97* (3), 493–497.
- 283 (4) Fitzgerald, G. *The Origins of Aerobiology and Airborne Disease Research in the United*  
284 *States, 1930-1955*. Intervals Podcast of the Organization of American Historians.  
285 <https://rebrand.ly/m0uxwym>.
- 286 (5) Mphaphlele, M.; Dharmadhikari, A. S.; Jensen, P. A.; Rudnick, S. N.; van Reenen, T. H.;  
287 Pagano, M. A.; Leuschner, W.; Sears, T. A.; Milonova, S. P.; van der Walt, M.; Stoltz, A. C.;  
288 Weyer, K.; Nardell, E. A. Institutional Tuberculosis Transmission. Controlled Trial of Upper  
289 Room Ultraviolet Air Disinfection: A Basis for New Dosing Guidelines. *Am. J. Respir. Crit.*  
290 *Care Med.* **2015**, *192* (4), 477–484.
- 291 (6) Greenhalgh, T.; Jimenez, J. L.; Prather, K. A.; Tufekci, Z.; Fisman, D.; Schooley, R. Ten  
292 Scientific Reasons in Support of Airborne Transmission of SARS-CoV-2. *Lancet* **2021**, *397*,  
293 1603–1605.
- 294 (7) Wang, C. C.; Prather, K. A.; Sznitman, J.; Jimenez, J. L.; Lakdawala, S. S.; Tufekci, Z.;  
295 Marr, L. C. Airborne Transmission of Respiratory Viruses. *Science* **2021**, *373* (6558),  
296 eabd9149.
- 297 (8) Morawska, L.; Tang, J. W.; Bahnfleth, W.; Bluysen, P. M.; Boerstra, A.; Buonanno, G.;  
298 Cao, J.; Dancer, S.; Floto, A.; Franchimon, F.; Haworth, C.; Hogeling, J.; Isaxon, C.;  
299 Jimenez, J. L.; Kurnitski, J.; Li, Y.; Loomans, M.; Marks, G.; Marr, L. C.; Mazzeo, L.;  
300 Melikov, A. K.; Miller, S.; Milton, D. K.; Nazaroff, W.; Nielsen, P. V.; Noakes, C.; Peccia, J.;  
301 Querol, X.; Sekhar, C.; Seppänen, O.; Tanabe, S.-I.; Tellier, R.; Tham, K. W.; Wargocki, P.;  
302 Wierzbicka, A.; Yao, M. How Can Airborne Transmission of COVID-19 Indoors Be  
303 Minimised? *Environ. Int.* **2020**, *142*, 105832.
- 304 (9) Jimenez, J. L. *GUV Cheat Sheet*. <http://bit.ly/guv-cheat>.
- 305 (10) J. B. Burkholder, S. P. Sander, J. Abbatt, J. R. Barker, C. Cappa, J. D. Crouse, T. S.  
306 Dibble, R. E. Huie, C. E. Kolb, M. J. Kurylo, V. L. Orkin, C. J. Percival, D. M. Wilmoth, and  
307 P. H. Wine. *Chemical Kinetics and Photochemical Data for Use in Atmospheric Studies*;  
308 JPL Publication 19-5; Jet Propulsion Laboratory, Pasadena, 2019.
- 309 (11) Claus, H. Ozone Generation by Ultraviolet Lamps†. *Photochem. Photobiol.* **2021**, *97* (3),  
310 471–476.
- 311 (12) Peng, Z.; Miller, S. L.; Jimenez, J. L. Model Evaluation of Secondary Chemistry due to  
312 Disinfection of Indoor Air with Germicidal Ultraviolet Lamps. *Environ. Sci. Technol. Lett.*  
313 **2023**, *10* (1), 6–13.
- 314 (13) Pagonis, D.; Price, D. J.; Algrim, L. B.; Day, D. A.; Handschy, A. V.; Stark, H.; Miller, S. L.;  
315 de Gouw, J.; Jimenez, J. L.; Ziemann, P. J. Time-Resolved Measurements of Indoor  
316 Chemical Emissions, Deposition, and Reactions in a University Art Museum. *Environ. Sci.*  
317 *Technol.* **2019**, *53* (9), 4794–4802.
- 318 (14) Liu, X.; Deming, B.; Pagonis, D.; Day, D. A.; Palm, B. B.; Talukdar, R.; Roberts, J. M.;  
319 Veres, P. R.; Krechmer, J. E.; Thornton, J. A.; de Gouw, J. A.; Ziemann, P. J.; Jimenez, J.  
320 L. Effects of Gas–wall Interactions on Measurements of Semivolatile Compounds and  
321 Small Polar Molecules. *Atmos. Meas. Tech.* **2019**, *12* (6), 3137–3149.
- 322 (15) Liu, X.; Day, D. A.; Krechmer, J. E.; Brown, W.; Peng, Z.; Ziemann, P. J.; Jimenez, J. L.  
323 Direct Measurements of Semi-Volatile Organic Compound Dynamics Show near-Unity  
324 Mass Accommodation Coefficients for Diverse Aerosols. *Commun. Chem.* **2019**, *2* (98), 1–

- 325 9.
- 326 (16) Krechmer, J. E.; Day, D. A.; Ziemann, P. J.; Jimenez, J. L. Direct Measurements of  
327 Gas/Particle Partitioning and Mass Accommodation Coefficients in Environmental  
328 Chambers. *Environ. Sci. Technol.* **2017**, *51* (20), 11867–11875.
- 329 (17) Krechmer, J.; Lopez-Hilfiker, F.; Koss, A.; Hutterli, M.; Stoermer, C.; Deming, B.; Kimmel,  
330 J.; Warneke, C.; Holzinger, R.; Jayne, J.; Worsnop, D.; Fuhrer, K.; Gonin, M.; de Gouw, J.  
331 Evaluation of a New Reagent-Ion Source and Focusing Ion–Molecule Reactor for Use in  
332 Proton-Transfer-Reaction Mass Spectrometry. *Anal. Chem.* **2018**, *90* (20), 12011–12018.
- 333 (18) Nazaroff, W. W. Residential Air-Change Rates: A Critical Review. *Indoor Air* **2021**, *31* (2),  
334 282–313.
- 335 (19) Keller-Rudek, H.; Moortgat, G. K.; Sander, R.; Sørensen, R. *The MPI-Mainz UV/VIS*  
336 *Spectral Atlas of Gaseous Molecules of Atmospheric Interest*.  
337 [http://satellite.mpic.de/spectral\\_atlas](http://satellite.mpic.de/spectral_atlas) (accessed 2022-02-10).
- 338 (20) Peng, Z.; Jimenez, J. L. KinSim: A Research-Grade, User-Friendly, Visual Kinetics  
339 Simulator for Chemical-Kinetics and Environmental-Chemistry Teaching. *J. Chem. Educ.*  
340 **2019**, *96* (4), 806–811.
- 341 (21) Blatchley, E. R.; Brenner, D. J.; Claus, H.; Cowan, T. E.; Linden, K. G.; Liu, Y.; Mao, T.;  
342 Park, S.-J.; Piper, P. J.; Simons, R. M.; Sliney, D. H. Far UV-C Radiation: An Emerging  
343 Tool for Pandemic Control. *Crit. Rev. Environ. Sci. Technol.* **2023**, *53* (6), 733–753.
- 344 (22) Ma, B.; Burke-Bevis, S.; Tiefel, L.; Rosen, J.; Feeney, B.; Linden, K. G. Reflection of UVC  
345 Wavelengths from Common Materials during Surface UV Disinfection: Assessment of  
346 Human UV Exposure and Ozone Generation. *Sci. Total Environ.* **2023**, 161848.
- 347 (23) Turner, M. C.; Jerrett, M.; Pope, C. A., 3rd; Krewski, D.; Gapstur, S. M.; Diver, W. R.;  
348 Beckerman, B. S.; Marshall, J. D.; Su, J.; Crouse, D. L.; Burnett, R. T. Long-Term Ozone  
349 Exposure and Mortality in a Large Prospective Study. *Am. J. Respir. Crit. Care Med.* **2016**,  
350 *193* (10), 1134–1142.
- 351 (24) Bell, M. L.; Peng, R. D.; Dominici, F. The Exposure–response Curve for Ozone and Risk of  
352 Mortality and the Adequacy of Current Ozone Regulations. *Environ. Health Perspect.* **2006**,  
353 *114* (4), 532–536.
- 354 (25) Weichenthal, S.; Pinault, L.; Christidis, T.; Burnett, R. T.; Brook, J. R.; Chu, Y.; Crouse, D.  
355 L.; Erickson, A. C.; Hystad, P.; Li, C.; Martin, R. V.; Meng, J.; Pappin, A. J.; Tjepkema, M.;  
356 van Donkelaar, A.; Weagle, C. L.; Brauer, M. How Low Can You Go? Air Pollution Affects  
357 Mortality at Very Low Levels. *Sci Adv* **2022**, *8* (39), eabo3381.
- 358 (26) Ma, B.; Gundy, P. M.; Gerba, C. P.; Sobsey, M. D.; Linden, K. G. UV Inactivation of SARS-  
359 CoV-2 across the UVC Spectrum: KrCl\* Excimer, Mercury-Vapor, and Light-Emitting-Diode  
360 (LED) Sources. *Appl. Environ. Microbiol.* **2021**, *87* (22), e0153221.
- 361 (27) Welch, D.; Buonanno, M.; Buchan, A. G.; Yang, L.; Atkinson, K. D.; Shuryak, I.; Brenner, D.  
362 J. Inactivation Rates for Airborne Human Coronavirus by Low Doses of 222 Nm Far-UVC  
363 Radiation. *Viruses* **2022**, *14* (4). <https://doi.org/10.3390/v14040684>.

364

## **Supporting Information for**

### **Significant Production of Ozone from Germicidal UV Lights at 222 nm**

Zhe Peng,<sup>1,2</sup> Douglas A. Day,<sup>1,2</sup> Guy Symonds,<sup>1,2</sup> Olivia Jenks,<sup>1,2</sup> Harald Stark,<sup>1,2,3</sup> Anne V. Handschy,<sup>1,2</sup> Joost de Gouw,<sup>1,2</sup> and Jose L. Jimenez<sup>1,2</sup>

1: Dept. of Chemistry, University of Colorado, Boulder, CO, USA

2: Cooperative Institute for Research in Environmental Sciences (CIRES), University of Colorado, Boulder, CO, USA

3: Aerodyne Research, Billerica, MA, USA

### **Supporting Information Text Sections**

#### ***Section S1. Selection and Application of CBr<sub>4</sub> a tracer of GUV fluence rate in air***

A useful chemical tracer of GUV exposure should not react (or react slowly) with common atmospheric oxidants such as O<sub>3</sub>, OH, or the NO<sub>3</sub> radical at typical indoor air concentrations. O<sub>3</sub> and NO<sub>3</sub> typically react only with C=C double bonds, while OH can abstract hydrogens from most organic molecules.<sup>1</sup> A tracer should also have a high absorption cross section at the most common GUV wavelengths (222 and 254 nm), so that its decay is large enough and can be quantified over reasonable time scales despite instrumental noise. It should have high vapor pressure and low water solubility to reduce partitioning to room surfaces and tubing.<sup>2,3</sup> It should not be highly toxic, and it should be detectable with high sensitivity with existing instrumentation, so that its mixing ratio can be kept low to minimize any unwanted effects on chemistry or human exposure concerns. After comparing a few candidate species, we selected CBr<sub>4</sub> as a tracer. We show that it has relatively fast decay under 222 nm irradiation and can be detected by a commonly-available Proton-Transfer-Reaction Mass Spectrometer with high sensitivity.

A search for species with these properties that can serve as a GUV fluence rate tracer at both main GUV wavelengths in use (222 and 254 nm) identified three candidates, shown in the table below. Other species considered (including CF<sub>2</sub>Br<sub>2</sub>, CCl<sub>3</sub>Br, CF<sub>2</sub>I<sub>2</sub>, C<sub>2</sub>F<sub>5</sub>I, CF<sub>3</sub>I, OCS, and diacetyl) had too low absorption cross section ( $\sigma$ ) at one of the key GUV wavelengths. CBr<sub>4</sub> was selected due to having the highest  $\sigma$  (and thus the fastest photolysis rates), low reactivity with oxidants, and being detectable with the Vocus instrument with high sensitivity. This instrument is widely-available in air chemistry research laboratories. This molecule is an excellent tracer in particular for GUV222, as its absorption cross section is highest at that wavelength, and falls about an order of magnitude when 10 nm away on either side of the peak. The absorption cross sections of CBr<sub>4</sub>, O<sub>2</sub> and O<sub>3</sub> are shown in Fig. S6.

To quantify the sensitivity of the Vocus to CBr<sub>4</sub>, 20.10 mg CBr<sub>4</sub> was evaporated under clean nitrogen flow into the chamber (whose volume was measured by quantitatively injecting CO<sub>2</sub> and measuring the concentration). A teflon-coated fan was run for one minute following the

addition to ensure complete mixing. The concentration of  $\text{CBr}_4$  in the chamber and measured ion counts per second (cps) for the  $\text{CBr}_3^+$  ion were used to determine the sensitivity in cps ppb<sup>-1</sup>.

As  $\text{CBr}_4$  also absorbs at 254 nm, it can cause interferences in the Thermo Scientific 49i  $\text{O}_3$  Analyzer, which uses absorption at 254 nm to measure  $\text{O}_3$ . We measured the apparent  $\text{O}_3$  signal in the Thermo Scientific 49i  $\text{O}_3$  Analyzer at several  $\text{CBr}_4$  concentrations in the absence of  $\text{O}_3$  in the chamber. Below 200 ppb  $\text{CBr}_4$ , the interference of  $\text{CBr}_4$  is approximately linear with its concentration (Fig. S11). The  $\text{O}_3$  signal due to  $\text{CBr}_4$  interference is  $\sim 0.007$  ppb per ppb  $\text{CBr}_4$  in this  $\text{CBr}_4$  concentration range, in which most of the experiments in this study were (usually on the range 1-10 ppb). At very high  $\text{CBr}_4$  concentration ( $\sim 500$  ppb), the relationship between the concentration and the  $\text{O}_3$  interference is no longer linear.

During the  $\text{O}_3$  generation rate quantification experiments,  $\text{CBr}_4$  (Sigma-Aldrich) was added to the chamber after the  $\text{O}_3$  quantification was done. This order was followed because  $\text{CBr}_4$  photolysis produces Br radicals that can catalytically destroy  $\text{O}_3$  in a similar way as catalytic destruction of stratospheric  $\text{O}_3$  by Cl.<sup>4</sup> In the presence of  $\text{CBr}_4$  and GUV irradiation (and hence Br atoms), a steady state for  $\text{O}_3$  exists that is governed by Br concentration (and hence  $\text{CBr}_4$  and GUV fluence rate). Fig. S12 shows the  $\text{O}_3$ - $\text{CBr}_4$  relationship during a long  $\text{CBr}_4$  decay experiment with the Far UV fixture (with filter).  $\text{CBr}_4$  decay was relatively slow. Therefore,  $\text{O}_3$  concentration responded to  $\text{CBr}_4$  relatively rapidly and could be regarded as steady-state concentration.

*Table S1. key properties of potential GUV average fluence rate tracers. (\*): Lifetimes are estimated for typical indoor GUV intensities of  $2.61 \times 10^{12}$  and  $1.06 \times 10^{14}$  photons  $\text{cm}^{-2} \text{s}^{-1}$  at 222 and 254 nm, respectively, and for an OH concentration of  $1.5 \times 10^6$  molec.  $\text{cm}^{-3}$ . (\*\*): no specific exposure limit, hazard information available at <https://pubchem.ncbi.nlm.nih.gov/>.*

Species	$\text{CBr}_4$	$\text{CHBr}_3$	$\text{BrCOC OBr}$	$\text{CF}_2\text{Br}_2$	$\text{CCl}_3\text{Br}$	$\text{CF}_2\text{I}_2$	$\text{C}_2\text{F}_5\text{I}$	$\text{CF}_3\text{I}$
$\sigma$ at 222 nm	2.85E-18	1.36E-18	2.00E-18	3.68E-19	4.60E-19	1.12E-18	4.73E-19	4.26E-19
$\sigma$ at 254 nm	1.32E-17	5.78E-18	7.00E-18	2.44E-18	4.80E-19	6.00E-19	2.48E-20	2.06E-20
OH rate coeff.	-	2.70E-13	-	-	-	-	-	-
GUV-222 lifetime* (h)	8.0	18.4	15.2	43.5	221.4	177.0	4284	5158
GUV-254 lifetime* (h)	0.9	1.9	1.3	7.1	5.7	2.3	5.6	6.2
OH lifetime* (h)	-	686	-	-	-	-	-	-
Exposure limit (ppb)	100	500	**	$10^5$	**	**	**	**

## Section S2. Selection of acetone as a tracer of Voc sensitivity

A Vocus sensitivity tracer was useful for some experiments with weak lamps, e.g. the Naomi Wu (portable) and Eden Park (B) devices (Table 1), where the  $\text{CBr}_4$  photolytic decay was small ( $\sim 0.01 \text{ h}^{-1}$ ) and the Vocus sensitivity drift could be of a comparable magnitude.

Acetone was selected as a tracer of Vocus sensitivity because of the following properties. First, the Vocus instrument detects acetone with high sensitivity.<sup>5</sup> Besides, its absorption cross section drops by orders of magnitude between 195-200 nm and is 3-4 orders of magnitude lower than that of  $\text{CBr}_4$  (Fig. S6), leading to little photolysis by the GUV band centered at 222 nm. Moreover, it is unreactive with  $\text{O}_3$ , and its reaction with OH is negligible under the conditions in this study. After injection into the chamber, the acetone signal can serve to continuously quantify small variations in Vocus sensitivity, for the experiments where the GUV device has the optical filter that filters the 190 nm band.

### **Section S3. Calibration of $\text{O}_3$ analyzers used for chamber and office experiments**

$\text{O}_3$  formation in the chamber was always measured with a Thermo Scientific 49i  $\text{O}_3$  Analyzer. That analyzer was calibrated using actinometry within the experimental chamber, where  $\sim 40$  ppb of  $\text{NO}_2$  was injected into the dry chamber, and the UVA lights are stepped through four discrete levels (between 10-100% of total UVA power). Equal amounts of NO and  $\text{O}_3$  are generated, which are monitored with the  $\text{O}_3$  analyzer and a Thermo Scientific 42i-TL  $\text{NO}-\text{NO}_2-\text{NO}_x$  Analyzer. The  $\text{NO}_x$  analyzer was calibrated using a NIST-certified ( $\pm 2\%$ ) calibration standard (gas cylinder with NO in  $\text{N}_2$ ) and Thermo Scientific Multi-Gas Calibrator (146i). We estimate that this method provides a calibration accuracy of  $\pm 5\%$  for the  $\text{O}_3$  analyzer.

$\text{O}_3$  decay rates and concentrations in the office experiments were always measured with a 2B Model 205 analyzer, which was cross-calibrated with the Thermo analyzer used in the chamber experiments, with its zero calibrated with zero air (resulting accuracy of  $\pm 7\%$ , and zero uncertainty of  $\pm 0.5$  ppb).

### **Section S4. Data analysis and kinetic modeling for the office $\text{O}_3$ production experiment**

#### *Characterization Tests*

In characterization tests (without a GUV lamp), the ventilation rate was measured as 0.52-0.61  $\text{hr}^{-1}$  ( $\tau$ : 1.6-1.9 h) using  $\text{CO}_2$  decay. For initial characterization of  $\text{O}_3$  decay,  $\sim 400$ -500 ppb  $\text{O}_3$  were generated with an unfiltered low-pressure Hg lamp with partial emission at 185 nm (BHK 82-9304-03) (Fig. S3), together with  $\text{CO}_2$  injection. As expected, the decay of  $\text{O}_3$  generated by the Hg lamp was faster than  $\text{CO}_2$  decay (Fig. S4), because of other  $\text{O}_3$  losses than ventilation (dry deposition, reactions with VOC emitted indoors etc.). Subtracting the two rate coefficients yields an  $\text{O}_3$  deposition coefficient of 0.76-1.1  $\text{h}^{-1}$  ( $\tau$ : 0.93-1.3 h), and the overall  $\text{O}_3$  decay rate as 1.3-1.7  $\text{hr}^{-1}$  ( $\tau$ : 0.59-0.78 h).

Given the variability in these experiments, the  $\text{CO}_2$  and  $\text{O}_3$  decay rates were measured after each period in which the GUV lamp was turned on, as described in the main paper.

## *Modeling*

To quantify the O<sub>3</sub> production rate from the GUV lamp, all relevant parameters affecting O<sub>3</sub> concentration in the office were modeled in KinSim. The first-order ventilation rate, first order deposition rate coefficient (implicitly including gas and aerosol reactions), and the approximate mixing ratio of O<sub>3</sub> entering the room from outside the room had to be measured or estimated.

The ventilation rate was directly measured using CO<sub>2</sub> pulse injection experiments discussed in the main paper, and the deposition rate was estimated by subtracting the ventilation rate from the first-order overall O<sub>3</sub> loss rate coefficient (green fit lines in Fig. S9). From here, the effective value for the O<sub>3</sub> mixing in from outside the room was approximated through tuning of the model when the lamp was off (blue points in Fig. S9). Finally, across 5 of the 8 peaks the production rate was tuned individually until it matched with each peak, and then the average was used as a constant production rate (individual values shown in Fig. S9 and used as a metric of uncertainty). Peaks 3, 7, and 8 were excluded due to rapidly changing O<sub>3</sub> background levels. As it was found that the estimated O<sub>3</sub> deposition rate varied substantially for the different light cycles, it was assumed to be constant for the model and the average value was used as an input (and computing “outside” O<sub>3</sub>). This choice was made since, given the relative invariability of the ventilation rate and lack of activity in the room, it seemed unlikely that actual O<sub>3</sub> deposition rate coefficient would change all that much. More likely, the variability was more driven by a combination of uncertainty in changing ventilation rates and “outside” O<sub>3</sub> on timescales faster than these parameters could be quantified, as well as the uncertainties associated with fitting and subtracting decay and ventilation rates. Figure S9 displays all of these parameters in the first “variable deposition” scenario as well as the second “constant deposition scenario”. The O<sub>3</sub> production rate for the GUV lamp was only calculated for the second scenario.

As seen in Fig. S10, The O<sub>3</sub> production rate for the conference room is slightly lower than that of the chamber due to the size of the room (~32.9 vs. ~20.6 m<sup>3</sup>) and effective UV pathlength (~3.2 vs. ~4.5 m). However, the results are within error bars when these differences are taken into account. The effective path length is shorter in the conference room both because of the shorter length of the room (3.8 m), and the combination with the narrowness of the room and furniture obstructions, which we estimate to reduce effective pathlength by ~15%.

### ***Section S5. Evaluation of handheld electrochemical O<sub>3</sub> monitors***

Three low-cost (~\$100) handheld electrochemical O<sub>3</sub> monitor models were compared with our research-grade UV absorption Thermo Scientific Model 49i Ozone Analyzer. Table S2 lists all three monitors with their relevant information and specs. Two identical monitors were tested for the Shenzhen Dienmern model.

**Table S2. Specifications for all low-cost O<sub>3</sub> monitors tested in the chamber instrument**

Company and cost	Name, Model, and Principle of Operation	Advertised Specifications	Resolution of Monitor Display
Shandong Renke Control Technology Co., Ltd.  \$114	“Portable Accurate O <sub>3</sub> Sensor”  Model: RS-MG41-O3  Electrochemical sensor	0~10.00 ppm  Accuracy: ±6%FS(@5ppm,25°C,50% RH)  Zero drift: ≤±1ppm  Duplicate Value: ≤2%  From listing on Renke’s website: <a href="https://www.renkeer.com/product/portable-ozone-meter/">https://www.renkeer.com/product/portable-ozone-meter/</a>	0.01 ppm (10 ppb)
Shenzhen Dienmern Testing Technology Co., Ltd  \$55	“Portable O <sub>3</sub> handheld gas analyzer”  Model: DM509-O3 model  Electrochemical sensor	O <sub>3</sub> (0-5 ppm)  From listing on Alibaba.com:  <a href="https://dienmern.en.alibaba.com/product/1600275994341-910743044/Portable-Ozone-Analyzer-Hing-accurate-O3-Ozone-sensor-Air-Detector-Intelligent-Sensor-Ozone-Meter-Air-Quality-Pollution-Monitor.html?spm=a2700.shop_index.111720.3.55b15bceN6NeQC">https://dienmern.en.alibaba.com/product/1600275994341-910743044/Portable-Ozone-Analyzer-Hing-accurate-O3-Ozone-sensor-Air-Detector-Intelligent-Sensor-Ozone-Meter-Air-Quality-Pollution-Monitor.html?spm=a2700.shop_index.111720.3.55b15bceN6NeQC</a>	0.001 ppm (1 ppb)
Shenzhen YuanTe Technology Co., Ltd  \$815	“Portable Gas Detector”  Model: SKY2000  Electrochemical sensor	0-10 ppm  Accuracy: ≤±3% F.S.  Repeatability: ≤±1%  Linearity Error: ≤±1%  Zero Shift: ≤±1% (F.S./year)  <a href="https://siafa.com.ar/media/src/sky2000-catalogue-with-datasheetam.pdf">https://siafa.com.ar/media/src/sky2000-catalogue-with-datasheetam.pdf</a>  <a href="https://www.ato.com/portable-o3-gas-detector?affiliate=shopping&amp;qclid=CjwKC_Aiwx_eiBhBGEiwA15qLN6lkKk3nanBn5ZAzfaL5ereQOHcjOLdUMcFdgNIEI_3Qk5t47it2RoCRVcQAvD_BwE">https://www.ato.com/portable-o3-gas-detector?affiliate=shopping&amp;qclid=CjwKC_Aiwx_eiBhBGEiwA15qLN6lkKk3nanBn5ZAzfaL5ereQOHcjOLdUMcFdgNIEI_3Qk5t47it2RoCRVcQAvD_BwE</a>	0.01 ppm (10 ppb)

The set up for these monitors in the chamber can be seen in Fig. S13. O<sub>3</sub> was injected into the chamber with a commercial O<sub>3</sub> generator (BMT 802N) periodically, followed by mixing with a fan, in order to generate constant concentration O<sub>3</sub> “steps”. The Thermo O<sub>3</sub> concentrations were logged continuously and the concentrations of the hand-held O<sub>3</sub> monitors were manually read and recorded for each step. The results of this comparison can be seen in Figs. S14 and S15.

Performance is very poor at the relevant levels for typical indoor O<sub>3</sub> and the levels expected when GUV222 is applied at e.g. ACGIH limits (i.e. no response for O<sub>3</sub> <150–400 ppb). At higher levels > 200 ppb, the Shenzhen YuanTe monitor eventually quantifies O<sub>3</sub> with good accuracy, while the other two models continue to be low by a factor of ~8. The Shenzhen YuanTe monitor is also distinct from the other two as it is a factor of ~10 more expensive. According to the information that we could find (see Table S2), two of these monitors appear to have failed their accuracy and/or zero drift specifications. For the other one, the only specs that we found were the measurement range and statements that it has high accuracy. To the best of our current knowledge, the lowest cost monitors capable of accurate O<sub>3</sub> measurements at single-digit or tens of ppb-level concentrations are based on UV absorption, and cost at least \$6000.

### Section S6. Comparison of the health effects (premature death) for O<sub>3</sub> and fine PM.

The mortality due to long-term exposure to O<sub>3</sub> (per unit mass of O<sub>3</sub>) can be estimated from the literature. Turner et al. (2016)<sup>6</sup> is considered the best study to date on this topic (J. Balmes, UCSF, pers. comm., 2023). This study reports an increase in all-cause mortality of 2% per 10 ppb increase in O<sub>3</sub>. 10 ppb are equivalent to 19.7 µg m<sup>-3</sup> at 1 atm and 298 K. Thus, we can estimate the risk per unit mass of O<sub>3</sub> as 2% / 19.7 = 0.10% per µg m<sup>-3</sup>.

For comparison, the mortality due to long-term exposure to PM<sub>2.5</sub> can be estimated from Figure 2a of Weichenthal et al. (2022)<sup>7</sup>. For their updated exposure function, the increased relative risk of mortality per unit increase in PM<sub>2.5</sub> (i.e. the slope of the curve) is highest between 2.5-4 µg m<sup>-3</sup>, at about 3.2% per µg m<sup>-3</sup>. At concentrations around the US PM<sub>2.5</sub> average of ~7 µg m<sup>-3</sup>, this value is 1% per µg m<sup>-3</sup> for their updated function, and 0.95% per µg m<sup>-3</sup> for the prior literature function.

Thus depending on the estimate used for PM<sub>2.5</sub> risk, the all-cause mortality risk of PM<sub>2.5</sub> is 9.5-32 times larger than for O<sub>3</sub>.

### References:

- (1) Atkinson, R.; Arey, J. Atmospheric Degradation of Volatile Organic Compounds. *Chem. Rev.* **2003**, *103* (12), 4605–4638.
- (2) Pagonis, D.; Price, D. J.; Algrim, L. B.; Day, D. A.; Handschy, A. V.; Stark, H.; Miller, S. L.; de Gouw, J.; Jimenez, J. L.; Ziemann, P. J. Time-Resolved Measurements of Indoor Chemical Emissions, Deposition, and Reactions in a University Art Museum. *Environ. Sci. Technol.* **2019**, *53* (9), 4794–4802.
- (3) Liu, X.; Deming, B.; Pagonis, D.; Day, D. A.; Palm, B. B.; Talukdar, R.; Roberts, J. M.; Veres, P. R.; Krechmer, J. E.; Thornton, J. A.; de Gouw, J. A.; Ziemann, P. J.; Jimenez, J. L. Effects of Gas–wall Interactions on Measurements of Semivolatile Compounds and Small Polar Molecules. *Atmos. Meas. Tech.* **2019**, *12* (6), 3137–3149.
- (4) Seinfeld, J. H.; Pandis, S. N. *Atmospheric Chemistry and Physics: From Air Pollution to Climate Change*; John Wiley & Sons, Inc.: Hoboken, NJ, USA, 2006; p 1232.
- (5) Pagonis, D.; Sekimoto, K.; de Gouw, J. A Library of Proton-Transfer Reactions of H<sub>3</sub>O<sup>+</sup> Ions Used for Trace Gas Detection. *J. Am. Soc. Mass Spectrom.* **2019**, *30* (7), 1330–1335.

- (6) Turner, M. C.; Jerrett, M.; Pope, C. A., 3rd; Krewski, D.; Gapstur, S. M.; Diver, W. R.; Beckerman, B. S.; Marshall, J. D.; Su, J.; Crouse, D. L.; Burnett, R. T. Long-Term Ozone Exposure and Mortality in a Large Prospective Study. *Am. J. Respir. Crit. Care Med.* **2016**, *193* (10), 1134–1142.
- (7) Weichenthal, S.; Pinault, L.; Christidis, T.; Burnett, R. T.; Brook, J. R.; Chu, Y.; Crouse, D. L.; Erickson, A. C.; Hystad, P.; Li, C.; Martin, R. V.; Meng, J.; Pappin, A. J.; Tjepkema, M.; van Donkelaar, A.; Weagle, C. L.; Brauer, M. How Low Can You Go? Air Pollution Affects Mortality at Very Low Levels. *Sci Adv* **2022**, *8* (39), eabo3381.
- (8) Claus, H. Ozone Generation by Ultraviolet Lamps†. *Photochem. Photobiol.* **2021**, *97* (3), 471–476.
- (9) Yoshino, K.; Esmond, J. R.; Cheung, A. S.-C.; Freeman, D. E.; Parkinson, W. H. High Resolution Absorption Cross Sections in the Transmission Window Region of the Schumann-Runge Bands and Herzberg Continuum of O<sub>2</sub>. *Planet. Space Sci.* **1992**, *40* (2), 185–192.
- (10) Burkholder, J. B.; Sander, S. P.; Abbatt, J. P. D.; Barker, J. R.; Cappa, C.; Crouse, J. D.; Dibble, T. S.; Huie, R. E.; Kolb, C. E.; Kurylo, M. J.; Others. *Chemical Kinetics and Photochemical Data for Use in Atmospheric Studies; Evaluation Number 19*; Pasadena, CA: Jet Propulsion Laboratory, National Aeronautics and Space ..., 2020. <https://trs.jpl.nasa.gov/handle/2014/49199>.

## **Supporting Information Figures**

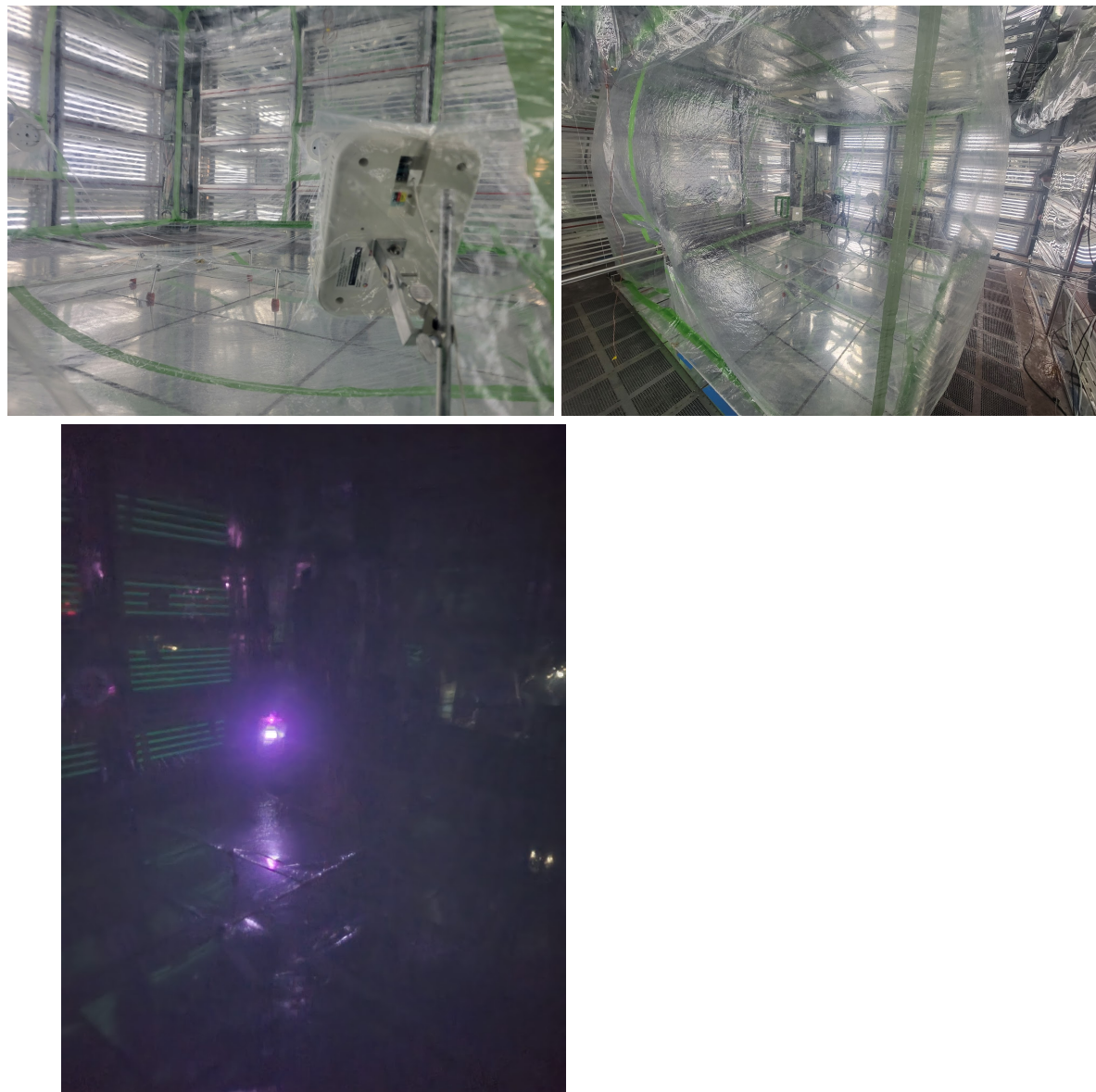


*Figure S1. Pictures showing the FarUV GUV222 lamp mounted inside the Teflon chamber. Other lamps were tested in the same physical configuration. All tests were performed with the visible lights off, as in the last picture.*

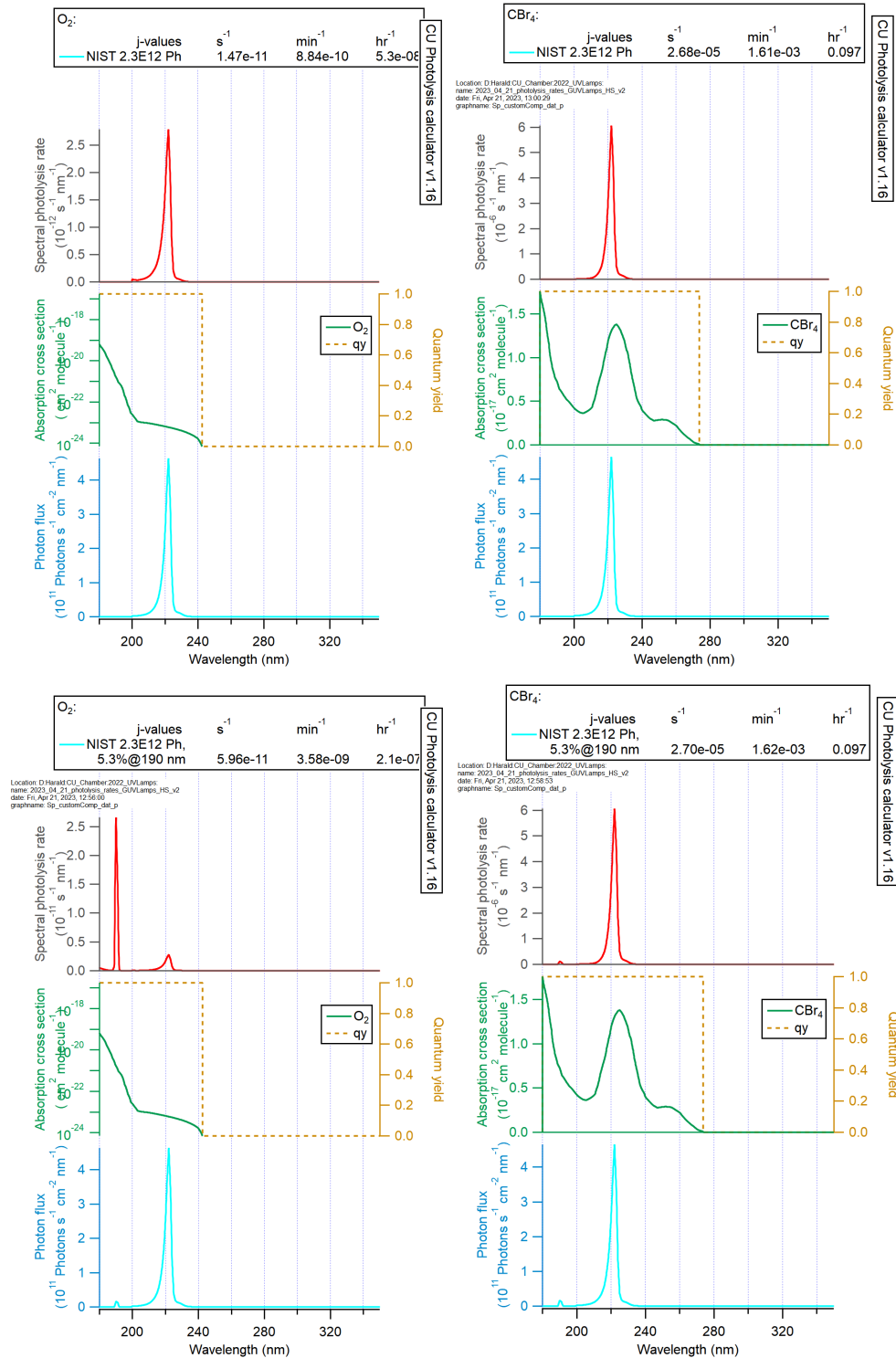
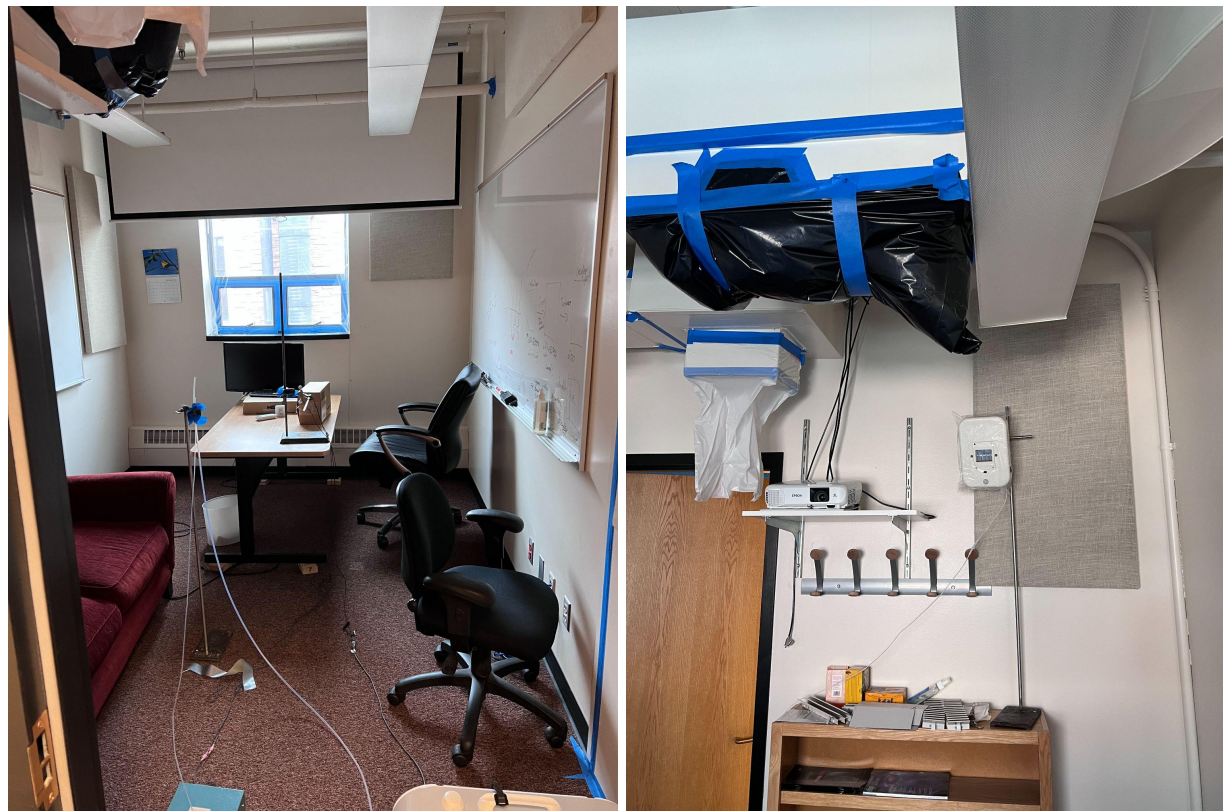
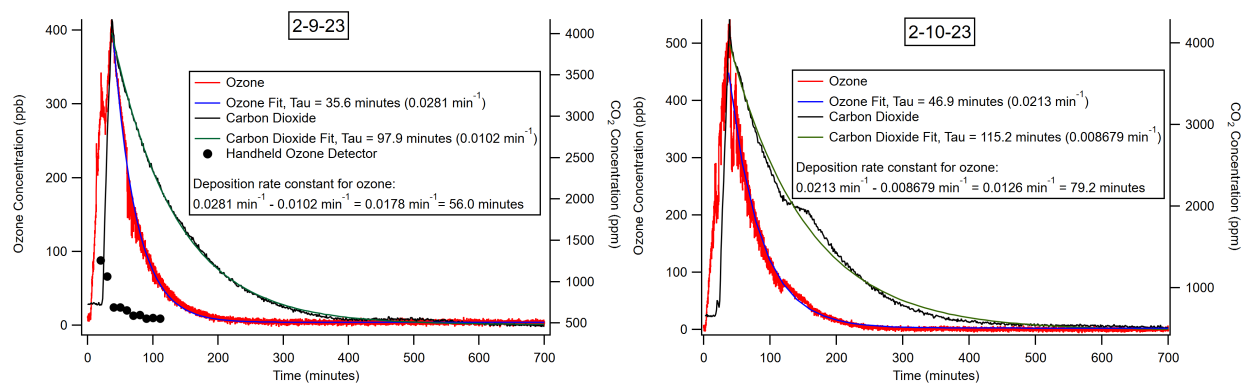


Figure S2. (Top) photolysis spectra and rates from O<sub>2</sub> (left) and CBr<sub>4</sub> (right) for NIST-measured Ushio lamp spectrum. (Bottom) results for the same lamp with an additional peak of 5.3% of the peak intensity manually added centered at 190 nm, estimated from Claus (2021).<sup>8</sup> These results were generated with the CU-Boulder photolysis calculator.



**Figure S3.** Experimental setup in the test office. The  $O_3$  sampling tube and  $CO_2$  injection tube were placed in the middle of the room on a ring stand (left). The GUV lamp was placed high in the room against the West wall of the room (right). The path of the light was interrupted by the furniture and walls, and the effective pathlength in the main paper was estimated to account for those obstructions.



**Figure S4.** Decays of  $O_3$  and  $CO_2$  in the office experiments, along with the approximate decay first-order rate coefficients for 2 experiments on 2 different days. Measurements from a handheld low-cost  $O_3$  detector are also shown, which underestimated the  $O_3$  concentration by about an order-of-magnitude (see Section S5).

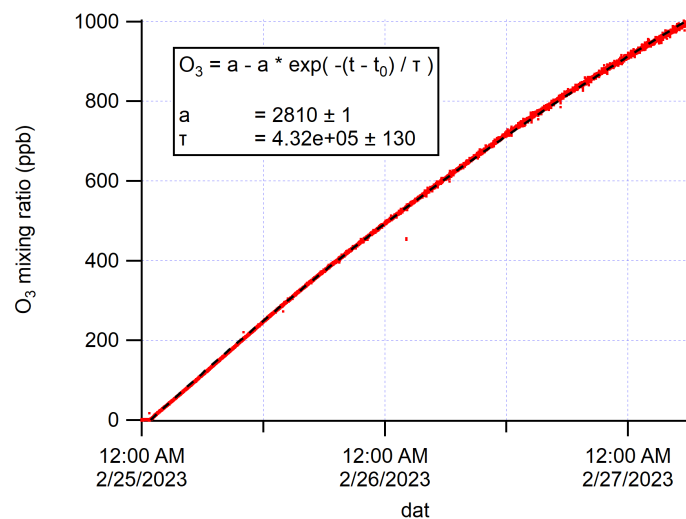


Figure S5. O<sub>3</sub> concentration vs. time in the chamber when the custom lamp with an Ushio B1 module was turned on for an extended period.

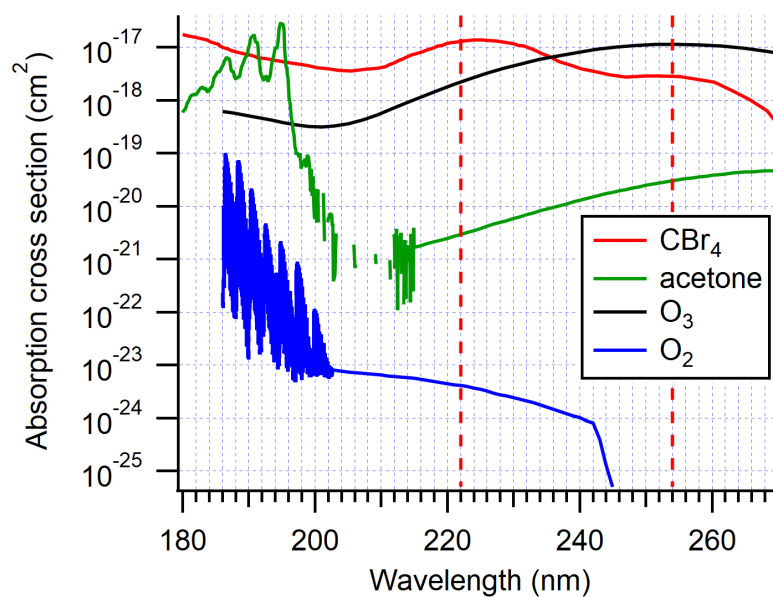
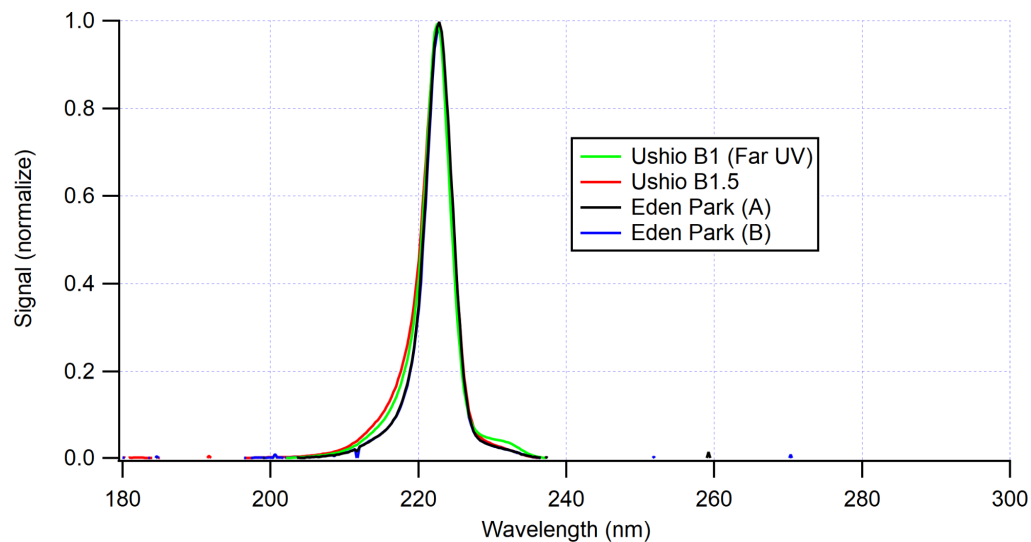
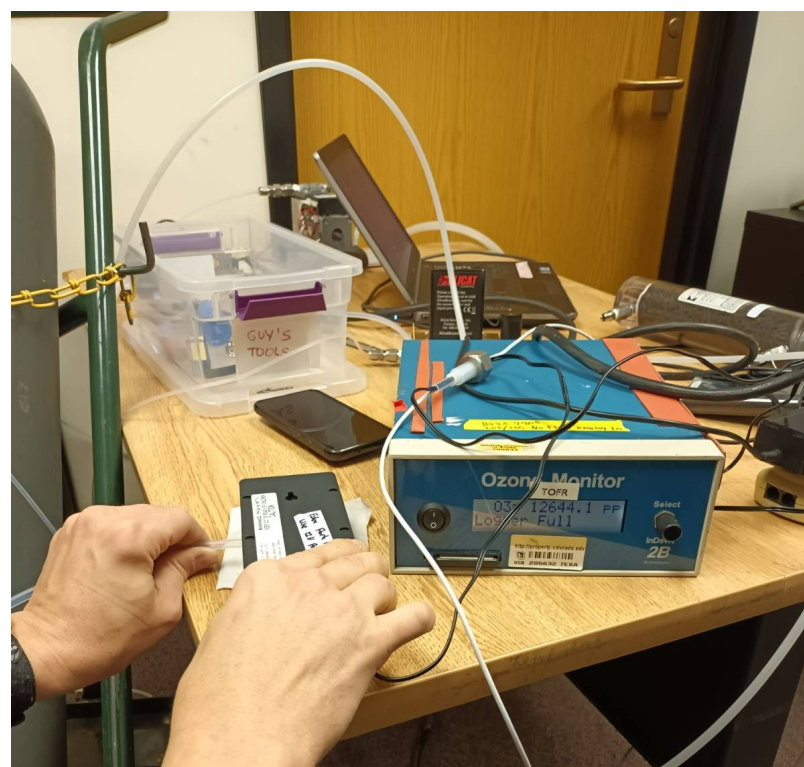


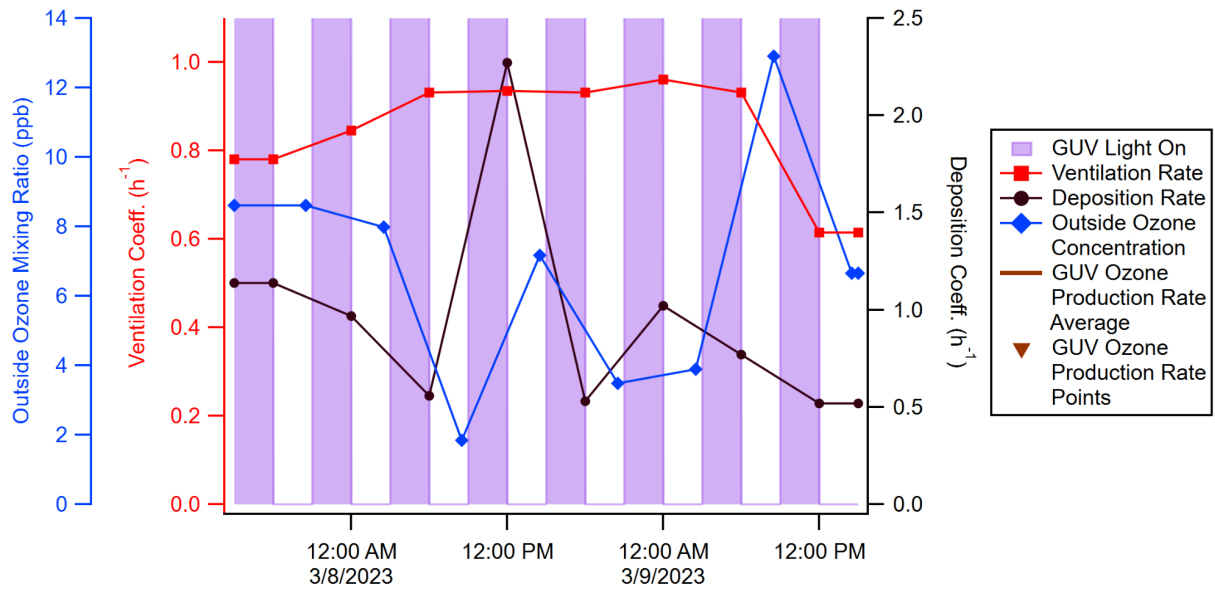
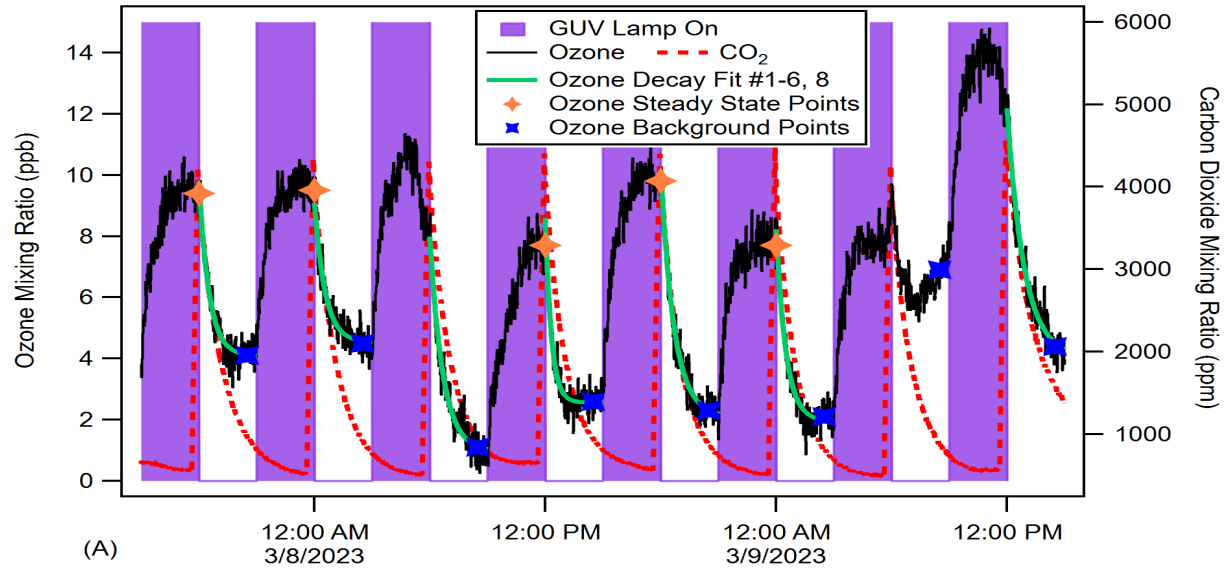
Figure S6. Absorption cross sections vs. UV wavelength for O<sub>2</sub>, O<sub>3</sub>, acetone and CBr<sub>4</sub>.<sup>9,10</sup>



*Figure S7. Measured emission spectra of the Far UV (Ushio B1), Ushio B1.5, and Eden Park (A) and (B) lamps. All spectra were measured with their original filters in place.*



*Figure S8. Picture of the setup for O<sub>3</sub> measurement just outside the electronics compartment of the Eden Park (A) device (black box held with right hand). The light emission surface points down into the table. The 2B O<sub>3</sub> analyzer displays a measured O<sub>3</sub> concentration of 12.6 ppm. Similar readings were observed for a period of several minutes.*



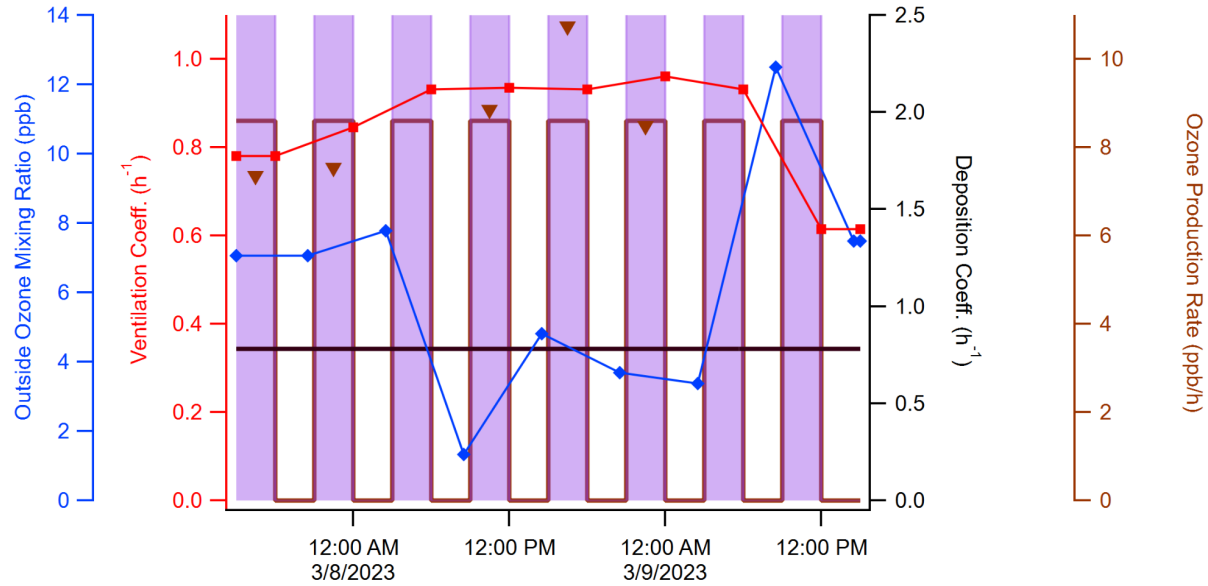


Figure S9. (Top):  $O_3$  concentration in the office as the GUV lamp was cycled on and off in 3-hour increments over 8 total cycles with corresponding  $CO_2$  pulses to measure ventilation rate. (Middle and Bottom): relevant parameters for modeling  $O_3$  concentrations in the office experiments with the KinSim model, plotted vs. time. The middle graph shows the scenario where deposition varies over time. The bottom graph shows the scenario where deposition is assumed to be constant.

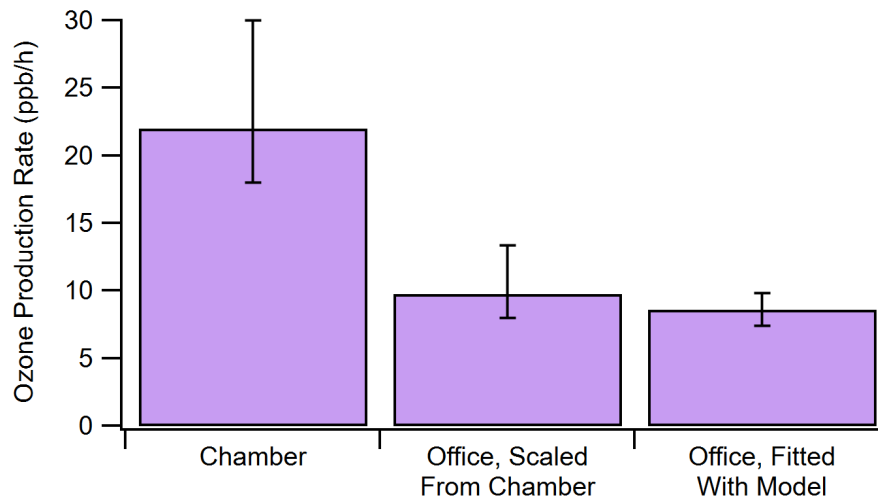


Figure S10. The production rates of  $O_3$  compared between the conference room and chamber along with the value expected for the conference room by scaling the chamber results with the relative room volume and effective GUV light pathlengths.

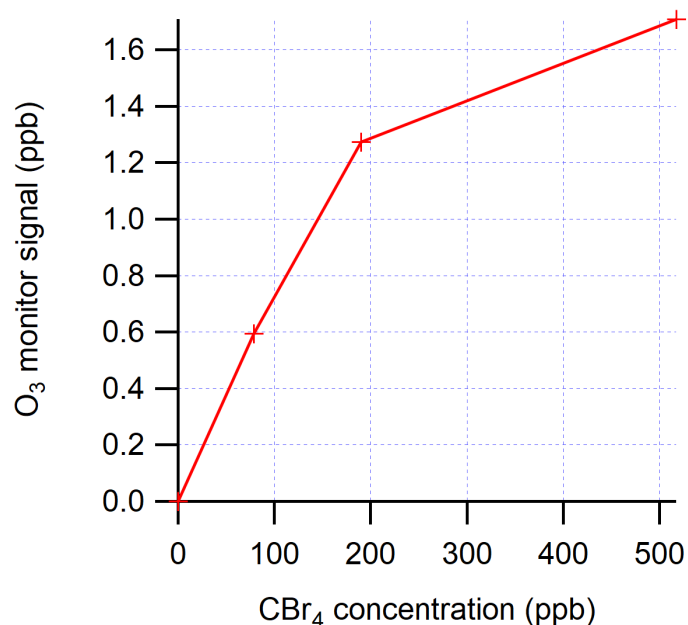


Figure S11. Apparent O<sub>3</sub> signal measured in the chamber due to CBr<sub>4</sub> interference at different CBr<sub>4</sub> concentrations.

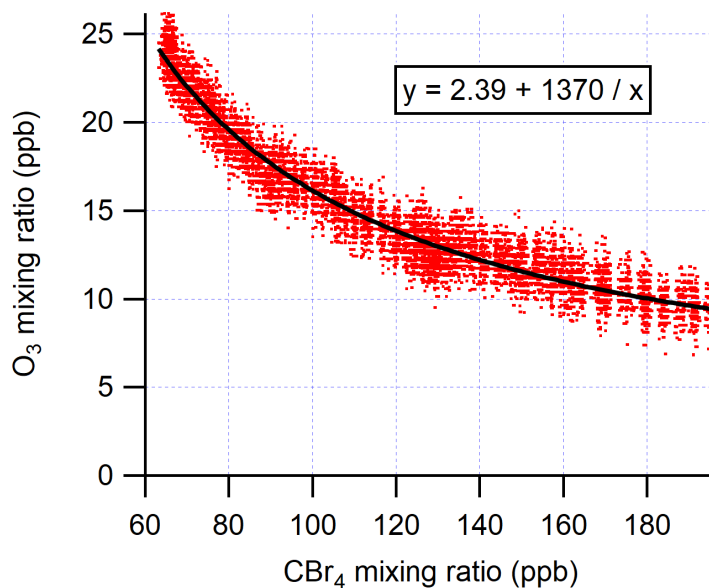
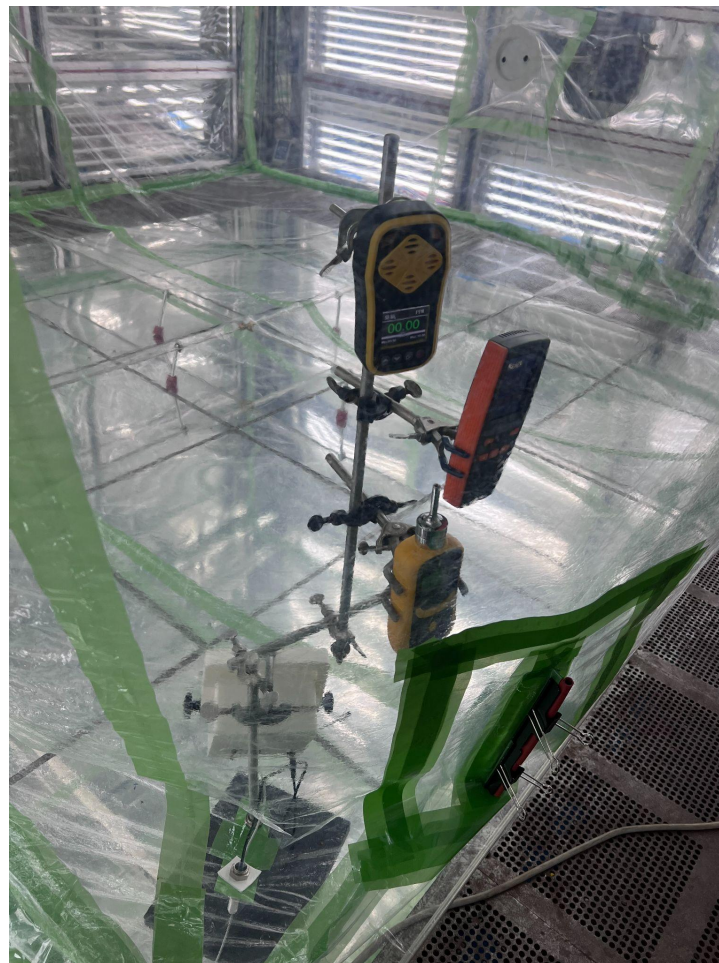


Figure S12. Evolution of O<sub>3</sub> and CBr<sub>4</sub> concentrations during a CBr<sub>4</sub> photolysis experiment with the Far UV lamp (Ushio B1) lasting 12 h.



*Figure S13. Set up with three handheld O<sub>3</sub> monitors inside of the chamber. The Shandong Renke model is on top, the Shenzhen Dienmern model is in the middle, and the Shenzhen YuanTe model is on the bottom.*

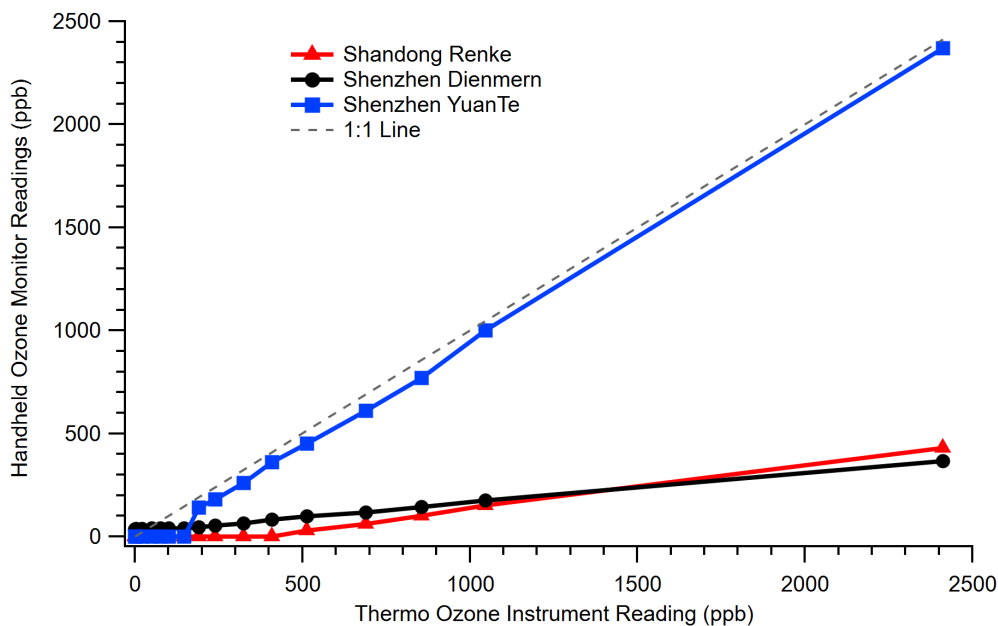


Figure S14. Comparison of the three portable  $O_3$  monitors against the research-grade Thermo  $O_3$  instrument.

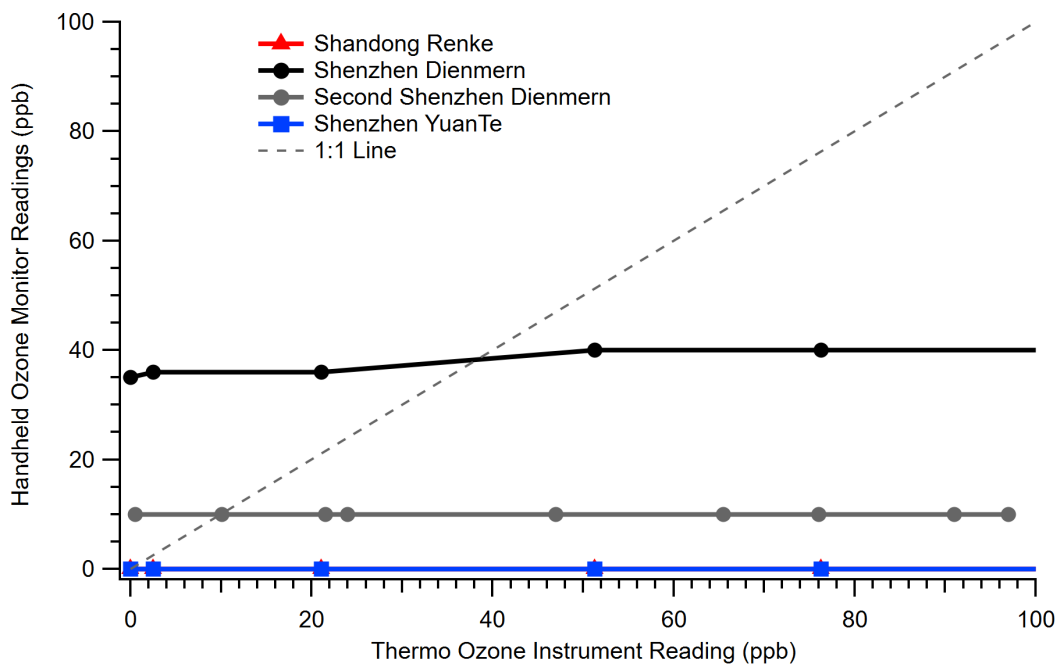


Figure S15. Comparison of the three portable  $O_3$  monitors against the research-grade Thermo  $O_3$  instrument, zoomed in the range of 0-100 ppb. A second and identical model Shenzhen Dienmern was also tested and shown in the gray line. This test was repeated once and none of the monitors showed appreciable differences, even the Shenzhen YuanTe still registered 0.00 ppm  $O_3$  (while being exposed to values in the range of this graph) after a zero calibration inside the clean  $O_3$ -free chamber.